Supporting Information

High-throughput fabrication of resonant metamaterials with ultra-small coaxial apertures via atomic layer lithography

*Daehan Yoo[1], Ngoc-Cuong Nguyen[2], Luis Martin-Moreno[3], Daniel A. Mohr[1], Sol Carretero-Palacios[4], Jonah Shaver[1], Jaime Peraire[2], Thomas W. Ebbesen[5], Sang-Hyun Oh[1,]**

[1]Department of Electrical and Computer Engineering, University of Minnesota, Minneapolis, Minnesota, 55455, U.S.A.

[2]Department of Aeronautics and Astronautics, Massachusetts Institute of Technology, Cambridge, Massachusetts, 02139, U.S.A.

[3]Instituto de Ciencia de Materiales de Aragón and Departamento de Física de la Materia Condensada, CSIC-Universidad de Zaragoza, E-50009 Zaragoza, Spain.

[4]Instituto de Ciencia de Materiales de Sevilla, CSIC-Universidad de Sevilla, 41092 Sevilla, Spain.

[5]ISIS, University of Strasbourg and CNRS, 67000 Strasbourg, France.

*E-mail: sang@umn.edu

Methods

Device fabrication. Polymethyl methacrylate resist (MicroChem, 950 PMMA C4) was spin-coated on a sapphire wafer (University Wafer), followed by sputtering of a 20-nm-thick aluminum layer (AJA, ATC 2200) to avoid charging during electron-beam lithography. Electron-beam lithography (VISTEC, EBPG5000+) was then performed at 100 keV beam energy and 1000 $\mu C/cm^2$ exposure dose to pattern a nanohole array. After removal of Al in a CD-26 solution, the exposed resist was developed by a solution of MIBK: IPA (1:3) for 90s. 3-nm Ti and 200-nm Au films were then directionally deposited on the patterned substrate using electron beam evaporator (CHA, SEC 600). After the lift-off process, oxygen plasma (STS, 320PC) was performed at 100W for 30s to remove resist residue. Next, an Al_2O_3 film was deposited on the Au nanopillar array using ALD (Cambridge Nano Tech Inc., Savannah) at a typical deposition rate of 1 Å per cycle at 250°C, followed by conformal deposition of a 400 nm Au film using an electron beam evaporator (CHA, SEC 600) with a planetary fixture. Finally, anisotropic ion milling (Intlvac, Nanoquest) was carried out by an Ar beam of 130 mA and 36 V incident at 10° from the horizontal plane for planarization.

Optical transmission measurements. For transmission measurements in the visible and NIR wavelengths, coaxial apertures were illuminated with a broadband fiber-coupled, laser driven light source (Energetiq, EQ-99FC) through a condenser on an inverted microscope (Nikon, Ti-S), and the light transmitted was collected with a 10X objective and imaged onto the entrance slit of a 300 mm focal length imaging spectrometer (Acton SP2300i) equipped with a CCD camera (Princeton, Pixis 400) for the visible and a thermoelectrically cooled, 256-element InGaAs diode array (BaySpec Nunavut) for the NIR. Spectra were background subtracted and normalized using the spectrum for direct transmission through the sapphire substrate.

FTIR instrument and measurement. The transmission spectra of coaxial apertures were measured in the MIR using Fourier transform infrared spectroscopy (Thermo Scientific, Nicolet Magna IR 750) with a transmission mode microscope. All of the data from coaxial aperture arrays were taken using the microscope with an unpolarized IR light source, a liquid-N_2-cooled MCT-A (Mercury ZincTelluride Alloy) detector, and an aperture size of 100 μm by 100 μm. The signals that were averaged for 256 times with a resolution of 4 cm^{-1} were normalized to the background signal taken from a bare sapphire wafer. The sapphire wafer was transparent up to 6.5 μm with measured transmittance of 80%.

AFM measurement. All AFM images were obtained with Veeco Nanoscope V multimode system. The samples were scanned using tapping mode, typically over a 2 x 2 μm area at a scan rate of 1 Hz. Nanoscope software was utilized to analyze the images and extract topographical information.

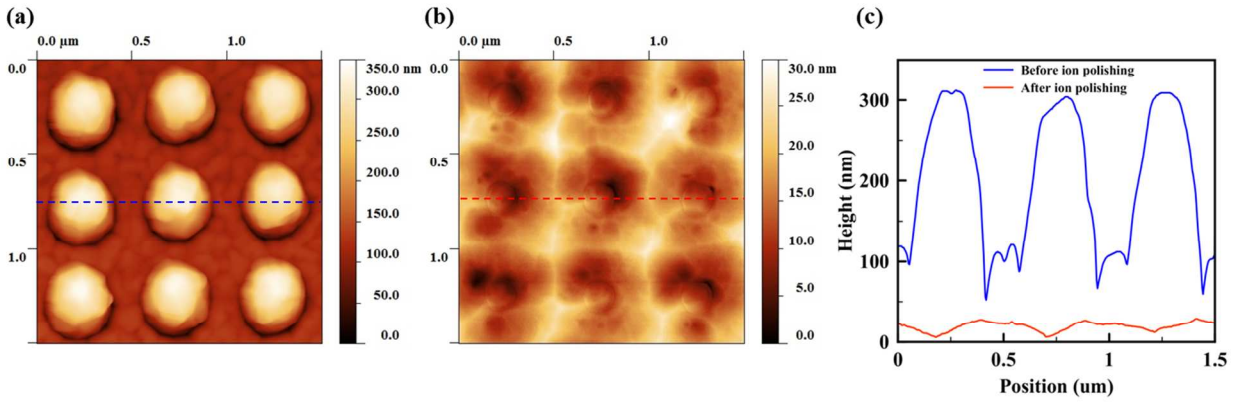

Figure S1. Atomic force microscope (AFM) characterization. (a) AFM 2-D image from the coaxial aperture array with 7 nm gap width, 150 nm diameter, and 500 nm period before glancing-angle ion milling. (b) AFM 2-D image from the coaxial aperture array with 7 nm gap width, 150 nm diameter, and 500 nm period after glancing-angle ion milling. (c) The comparison of 1-D height profiles over a dashed line in AFM images before and after glancing-angle ion milling.

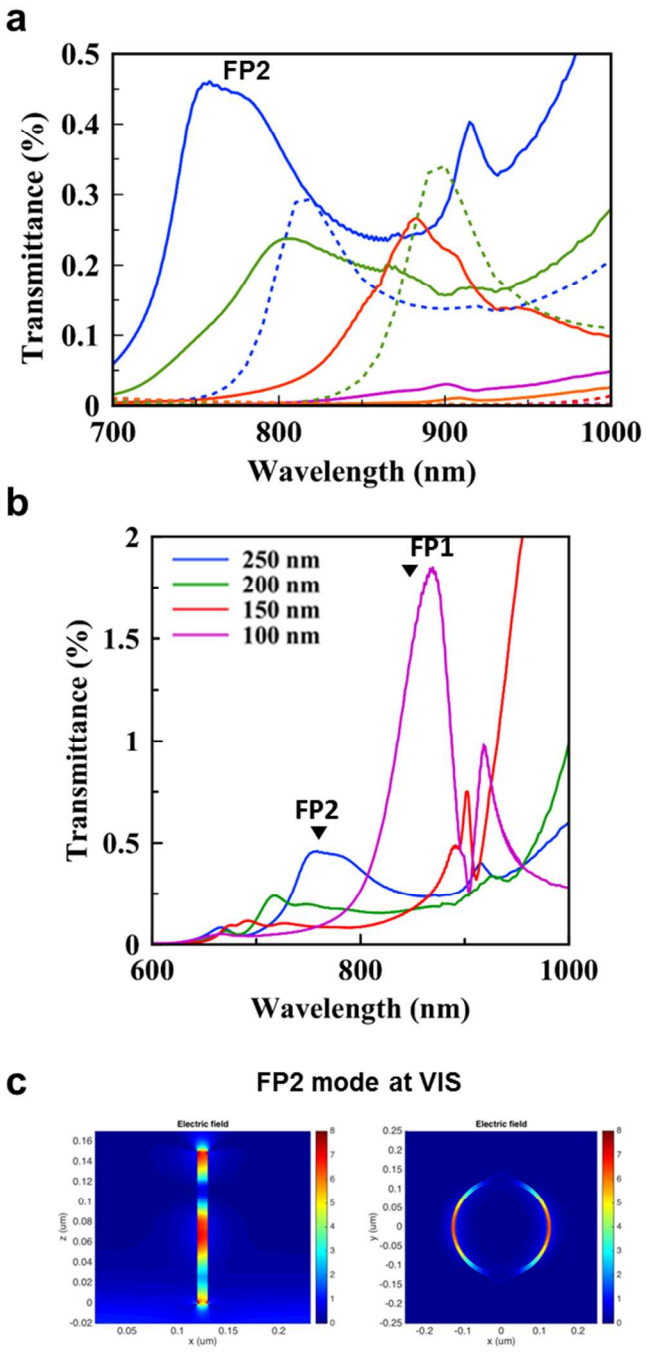

Figure S2. (a) The measured and simulated NIR spectra of light transmitted from the coaxial aperture array with a 250 nm diameter and five different gap widths (1, 2, 4, 7, 10 nm). (b) The measured visible and NIR spectra of light transmitted from the coaxial 10-nm gap with 100, 150, 200, 250 nm diameters. (c) Calculated electric field distributions of a 250 nm diameter coaxial aperture with a 10 nm gap at the resonance wavelength of 750 nm.

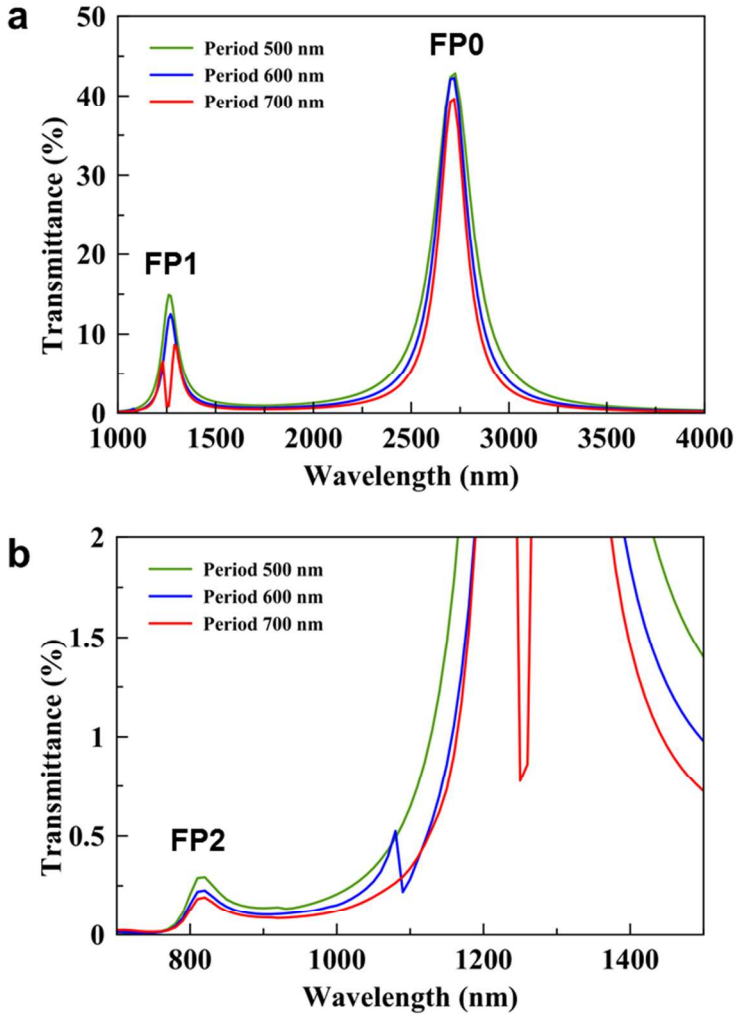

Figure S3. The effect of period on the transmission resonances excited from coaxial aperture arrays: (a), (b) 3D HDG FEM simulation of light transmitted from a coaxial aperture with a 10-nm-wide gap, 250 nm diameter and 500, 600, 700 nm period. Zeroth-order mode (FP0), FP1, and FP2 show no dependence on the array period. As the period increases, Wood's anomaly redshifts and leads to a Fano resonance when it overlaps with the FP1 mode.

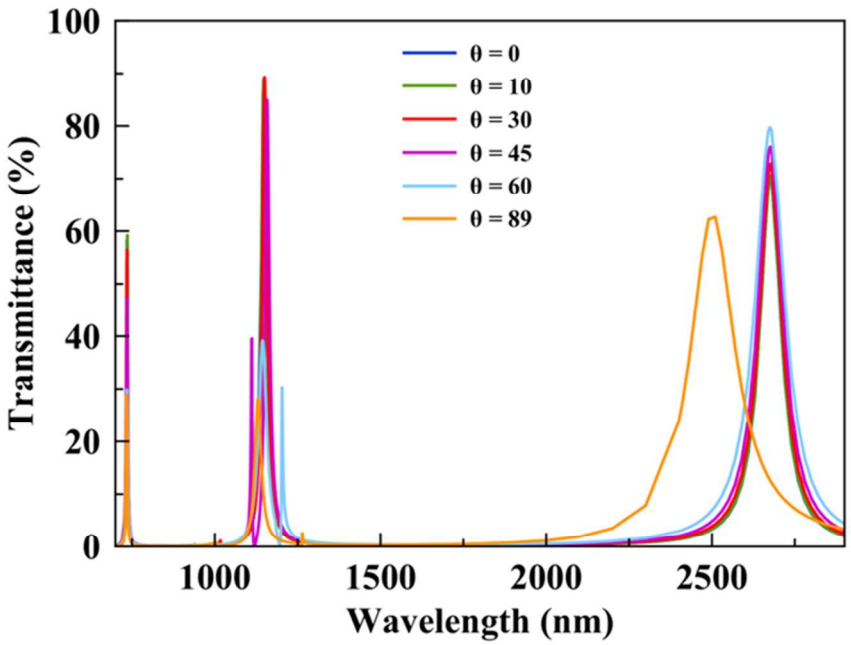

Figure S4. The angular dependence on the transmission resonances excited from the coaxial aperture array. CMM modeling of light transmitted from the coaxial 10-nm-wide gap with 250 nm diameter by different incident angles of light. Zeroth-order mode (FP0), FP1, and FP2 show no dependence on the incident angles.

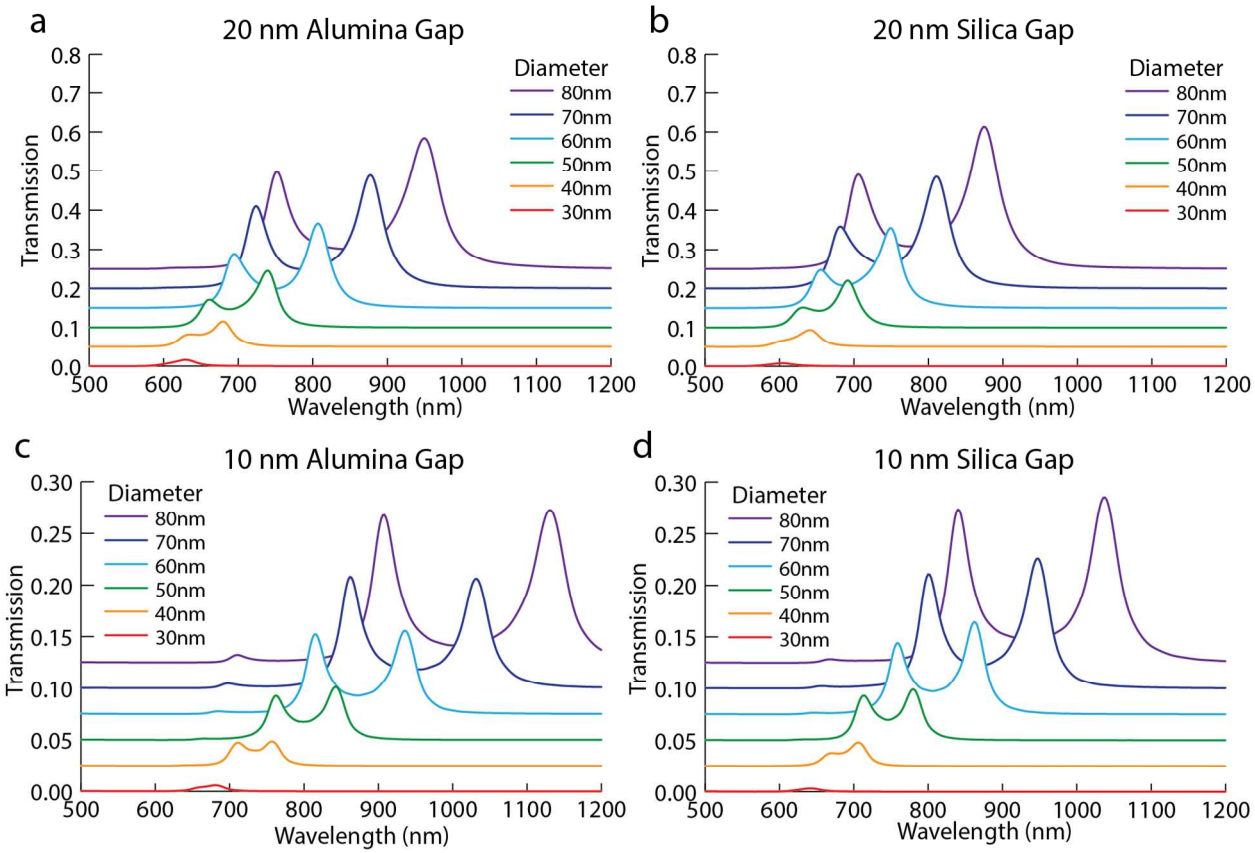

Figure S5. Finite-difference time-domain (FDTD) simulation of decreasing coaxial aperture diameter demonstrating FP0 resonances in the visible regime. As expected, when a dielectric material with a lower refractive index than alumina (e.g. silica) is deposited by atomic layer deposition, resonances blue-shift for equivalent device parameters. (a,b) Comparison of resonances for alumina- and silica-filled coaxial apertures with a 20 nm gap size. (c,d) Same as (a,b), except with a 10 nm gap size. All coaxial apertures were simulated to be through a 150 nm gold film with a 300 nm periodicity on a glass substrate. FDTD modeling was performed in Lumerical FDTD Solutions.

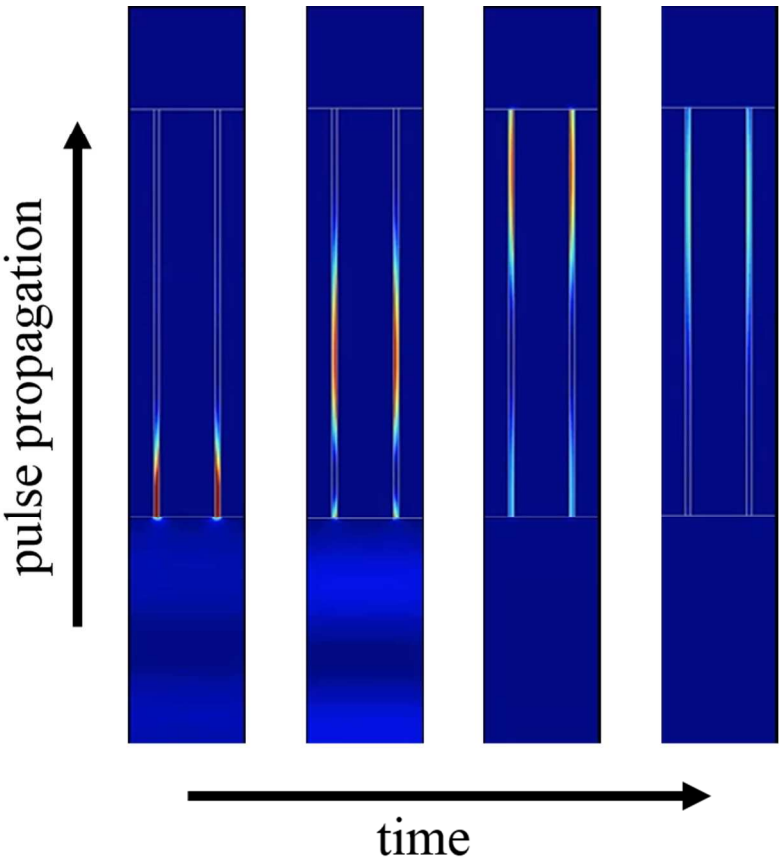

Movie (Figure as stand-in): FDTD simulation in full 3D of the "slow-light" mode in a 250 nm diameter Au coaxial aperture with a 20nm gap. Illumination is from below by a 66 fs pulse with a center wavelength of 2.5 μm and a 140 nm bandwidth. As the pulse enters the waveguide, the group velocity greatly decreases, while the dispersion of the cavity lengthens the pulse in duration. The length of the coaxial waveguide is 2 μm to emphasize the slow-light effect. (For the images) The time points shown were chosen to emphasize the effect.

Table S1. The comparison of the nominal and measured thickness of ALD-grown Al_2O_3 thin-film. For the convenience, all graphs were plotted with the nominal gap widths, while the measured gap widths were used for all numerical and analytical calculations.

Nominal gap width (nm)	Measured gap width (nm)
10	10.2
7	7.6
4	4.5
2	2.3